Parenchymal CSF fraction is a measure of brain glymphatic clearance and positively associated with beta-amyloid deposition on PET

Liangdong Zhou [1], Thanh D Nguyen [2], Gloria C Chiang [1,3], Xiuyuan H Wang [1], Ke Xi [1], Tsung-Wei Hu [1], Emily B Tanzi [1], Tracy Butler [1], Mony de Leon [1], Yi Li [1]

Abstract

Propose: Glymphatic clearance deficits has been postulated to lead to Aβ deposition in Alzheimer's disease, and can be reflected in dilation of perivascular space (PVS). Mapping of microscopic changes in the PVS of the cerebral cortex, beyond visible PVS in white matter, may enhance our ability to diagnose AD early and advance our understanding of disease etiology.

Methods: We used the CSF water fraction (CSFF), an MR-based biomarker derived from multi-echo FAST-T2 data and a three-water compartmental model, to characterize brain parenchymal CSF water, reflecting of microscopic PVS in parenchyma. We measured CSFF and Aβ using ^{11}C-PiB PET to investigate their relationship at both the subject and voxel level using multivariate regression analysis. We tested the effect of gender on all variables in selected regions of interest (ROI). We also evaluated the difference in CSFF among diagnostic groups.

Results: The results in 21 subjects (14 CN and 7 with MCI/AD, 6 male, 15 female, age: 66.62 ± 12.85) show that parenchymal CSFF is significantly associated with Aβ deposition ($t = 5.355$, $p < 0.0001$, $R^2 = 0.609$) at subject level when controlling for age and gender. Furthermore, regional CSFF in the Aβ+ subregion of posterior cingulate cortex (PCC) is elevated compared with that in the Aβ- subregion ($p < 0.01$) in CN subjects.

Conclusion: Our results show that an increased CSFF is associated with Aβ deposition, suggesting that CSFF could serve as a biomarker for brain glymphatic clearance, which can be used to detect early fluid changes predisposing individuals to the development of AD.

Author affiliations:

1 Department of Radiology, Brain Health Imaging Institute (BHII), Weill Cornell Medicine, 407 E 61st St, New York NY 10065, United States

2 Department of Radiology, MRI Research Institute (MRIRI), Weill Cornell Medicine, 407 E 61st St, New York NY 10065, United States

3 Department of Radiology, Division of Neuroradiology, Weill Cornell Medicine, NewYork-Presbyterian Hospital, 525 East 68th Street, Starr Pavilion, Box 141, New York NY, 10065, United States

Correspondence author: Yi Li, Ph.D., M.D.

Department of Radiology, Brain Health Imaging Institute, Weill Cornell Medicine

407 E 61st St Feil-206, New York NY 10065, United States

E-mail: yil4008@med.cornell.edu

Running title: CSF fraction associates with Aβ deposition

Keywords: CSF fraction; glymphatic clearance; beta amyloid; Alzheimer's disease; positron emission tomography, magnetic resonance imaging

Abbreviations: Aβ = beta-amyloid; AD = Alzheimer's disease; CN = cognitively normal; CSFF = CSF fraction; GM = cerebral cortex; IEWF = intra-extracellular water fraction; MCI = mild cognitive impaired; MWF = myelin water fraction; PVS = perivascular space; PVE = partial volume effect; PCC = posterior cingulate cortex; PiB = Pittsburgh compound B; ROI = region of interest; SUVR = standardized uptake value ratio; WM = cerebral white matter.

Introduction

Glia-lymphatic (Glymphatic) clearance deficits have recently gained attention as a major driver of the amyloid pathology seen in neurodegenerative conditions like Alzheimer's disease (AD) [1,2]. Perivascular spaces (PVS) in the brain contain CSF-like fluid and constitute a key component of glymphatic clearance. Specifically, PVS enlargement is believed to reflect reduced CSF flow and impaired glymphatic clearance [3]. This dysfunctional CSF clearance can lead to the deposition and accumulation of extracellular amyloid beta (Aβ) plaques that can be quantified using positron emission tomography (PET) with various radiotracers [1,4,5]. Historically, PVS load has been associated with an array of conditions and has been quantified using T2-weighted MRI and image segmentation techniques. Limitations of PVS segmentation approaches include image quality and resolution, and also low detection of PVS at the sub-voxel level or within close proximity to arteries and veins [6–8]. We developed a three-compartment water model to characterize fluid within the brain, using multi-echo MR T2 relaxometry to quantify the parenchymal CSF fraction (CSFF), the intra-extracellular water fraction (IEWF) and the myelin water fraction (MWF) [9,10]. According to biophysical principles, CSFF is the component of the total T2 signal with a long T2 time (T2 > 200ms in 3T magnetic field) that theoretically corresponds to the freely mobile water that resides in the PVS [11,12]. Therefore, since PVS is a component of the glymphatic system, CSFF could serve as a biomarker of glymphatic clearance. Our previous study showed that the CSFF quadratically increases in cerebral cortex (GM) and linearly increases with normal aging in deep gray matter (dGM) and cerebral white matter (WM), suggestive of decreased glymphatic function or more retention of glymphatic fluid in PVS and parenchyma with age [13]. Research on water homeostasis is not only important to healthy aging, but also the understanding of the progression of neurodegenerative disease. For example, CSF clearance in lateral ventricle has been shown to be associated with AD pathology [5,14]. Thus, changes in CSF in tissue (CSFF)

could be sensitive enough to detect subtle developments in pathology and serve as an early diagnostic biomarker [13]. This lead us to further investigate the relationship between CSFF and established AD markers such as Aβ deposition, and to investigate whether AD status could be sufficiently inferred using CSFF data [15].

In this study, we assessed the relationship between CSFF and brain Aβ deposition measured by ^{11}C-PiB PET in patients with mild cognitive impairment (MCI) or mild AD, and cognitively normal (CN) control subjects. We evaluated the effects of age and diagnostic group on CSFF. We specifically investigated the regional distribution of CSFF in the Aβ positive and negative voxels of the posterior cingulate cortex (PCC), a widely accepted region of early Aβ deposition in AD [16–18]. We hypothesized that increased CSFF would be associated with diagnostic group and regional Aβ deposition.

Materials and methods

Subjects

In this cross-sectional study a total of 29 of subjects had both MR-based CSFF maps and 11C-PIB PET scans. Seven subjects diagnosed with MCI that were Aβ negative (PiB PET reading) and excluded, as was one with multiple sclerosis (MS), leaving 21 eligible subjects. 7 of the 21 subjects were diagnosed as MCI/AD and 14 were CN. All studies were approved by the WCM Institutional Review Board (IRB) and written informed consent was obtained from all participants.

Subject assessment

All subjects underwent standardized evaluations by a cognitive neurologist. The evaluation consisted of neurological exam, interviews with subject and informant, Clinical Dementia Rating Scale (CDR) [19], MOCA [20], the NACC Uniform Data Set V3.0 telephone cognitive battery [21], clinical blood tests, ECG, MRI, amyloid (^{11}C-PiB) and tau (^{18}F-MK-6240) PET scanning. Subjects were assigned a final diagnosis by a board-certified neurologist (T.B.) in accordance with NACC criteria based on evaluation of all available information. The MRI and PET examinations were reviewed by a board-certified radiology with subspecialty certification in neuroradiology and 14 years of experience in diagnostic brain PET imaging (G.C.). All subjects were reviewed in a multidisciplinary consensus conference. Subjects included in this study were diagnosed as either cognitively normal (CN) or with mild cognitive impairment or mild dementia due to AD (MCI/AD).

Image acquisition

MRI images acquisition

All subjects underwent brain MRI studies on a Siemens Prisma 3T scanner (Siemens Healthineers, Erlangen, Germany) using a product 64-channel head/neck receiver coil. The brain imaging protocol consisted of 3D MPRAGE T1w and 3D T2SPACE sequences for anatomical structural imaging, as well as 3D FAST-T2 sequence for mapping of water fractions (WF), and T2 FLAIR sequence for WM hyperintensity detection [9]. The imaging parameters were as follows[13,22]: (1) 3D sagittal T1 MPRAGE: TR/TE/TI = 2,300/2.3/900 ms, flip angle (FA) = 8°, readout bandwidth (rBW) = 200 Hz/pixel, voxel size = 1.0 mm isotropic, GRAPPA parallel imaging factor (R) = 2, scan time = 5.5 min, (2) 3D sagittal T2W SPACE: TR/TE = 3,200/408 ms, FA = 90°, rBW = 751 Hz/pixel, turbo factor = 285, voxel size = 1.0 mm

isotropic; (3) 3D axial FAST-T2 at two slice thickness: spiral TR/TE = 7.8/0.5 ms, nominal T2prep times = 0 (T2-prep turned off), 7.5, 17.5, 67.5, 147.5, and 307.5 ms, FA = 10°, rBW = 1,042 Hz/pixel, number of spiral leaves per stack = 32, number of spiral leaves collected per T2prep = 64, voxel size = 1.3x1.3x2 mm3 (scan time = 7 min); (4) 3D sagittal FLAIR SPACE with fat saturation: TR/TE/TI = 4,000/384/2,400 ms, echo spacing = 3.46 ms, FA = 90°, rBW = 751 Hz/pixel, turbo factor = 278, voxel size = 1.0 mm isotropic, R = 2, scan time = 5.4 min.

PET images acquisition

11C-PiB PET image was acquired using a Siemens Biograph mCT–S (64) slice PET/CT. 11C-PiB was synthesized by the institutional radiochemistry facility. The data was acquired in list mode from 40-90 min after rapid bolus injection of ~555 MBq. PiB PET images were reconstructed to a 512 × 512 × 74 matrix of 0.8 × 0.8 × 3 mm voxels in 5 x 10 min time frames from 40 min to 90 min with list mode.

Image processing

MRI ROI parcellation

T1w MRI was regionally segmented using FreeSurfer (FS) [23] version 7.1 recon-all command for ROI parcellation with the assistance of T2w to enhance segmentation quality. ROIs consisted of bilateral cerebellar cortex as a reference region for Aβ SUVR determination, and an ROI encompassing the bilateral parietal, frontal and temporal ROI, were collectively referred to as the AD cortical mask (ADmask) for quantifying Aβ [16]. ROIs for CSFF values included: ADmask and posterior cingulate cortex (PCC) were extracted from FS aparc+aseg segmentation file matched with FS look-up-table (LUT). To reduce PVE, all ROIs for CSFF calculation were eroded according to the image resolution. Specifically, for CSFF, the ROI anisotropic erosion was done with gaussian kernel sized 1.3x1.3x2 mm3. All ROIs for PET

SUVR calculation were eroded by one voxel using 3D sphere kernel to minimize partial volume effect.

PET SUVR

Summed PiB PET data from 60 min to 90 min were used for SUVR calculation. Specifically, all the dynamic frames were realigned to the summed images between 40-90min, and the summed image was then coregistered to the T1w in FS space using normalized mutual information method in FSL.[24] SUVR was calculated using the cerebellar cortex as a reference region [25]. Average SUVR within the cortical ADmask served as the overall measure of Aβ deposition [16].

At the voxel level, PCC Aβ+ and Aβ- voxels were defined by using SUVR cut-off 1.6, and combined to form ROIs denoted as AβpROI and AβnROI, respectively [26,27]. AβpROI and AβnROI were then intersected with PCC, respectively, to get finalized AβpROI and AβnROI for CSFF values calculation.

CSFF mapping

CSFF, IEWF and MWF maps were obtained using nonlinear least square fitting of the 3-exponential model with L2 regularization. The input data of the fitting process was the 6 echo FAST-T2 data with degibbs and denoising processing. CSFF is the component corresponding to long T2 (T2>200 ms) signal and was constrained in the fitting process. The details of the mapping procedure was documented in our previous publications [9,13]. The CSFF mapping in this study was done identically with the same in-house processing pipeline. The water maps were rigidly coregistered to FS T1w space using normalized mutual information criteria. The ROI values of CSFF were extracted by averaging the CSFF in all the voxels of the ROI.

Statistical analysis

Statistical analyses were performed in RStudio Version 2022.7 (RStudio PBC) and MATLAB Version 2023a (MathWorks). First, we tested gender differences in the continuous variables like CSFF, PiB SUVR, age, using Wilcoxon rank sum test, and of binary variables like diagnostic group and Aβ status using Pearson's Chi-square test. Second, we performed the subject level analysis of the relationship between CSFF and PiB SUVR in ADmask using linear regression by controlling for age and gender. Third, we evaluated the association between CSFF and age in both CN and MCI/AD group using multivariable regression analysis controlling for gender. Independent two-sample t-test was used to test difference of CSFF between CN and MCI/AD subjects. Fourth, we performed the tests of regional CSFF distribution in Aβ+ and Aβ- subregions of PCC using paired Wilcoxon Rank Sum test. The significant level of all tests and analyses was set to $p<0.05$.

Data availability

Raw data were generated at the Brain Health Imaging Institute at Weill Cornell Medicine. Derived data supporting the findings of this study are available from the corresponding author on request.

Results

Subject information

The subjects' demographic and clinical information is listed in Table 1. The last column in Table 1 is the p-value for each measure compared by diagnostic group. Among the 21 subjects, there were 10 Aβ+ and 11 Aβ- subjects. Among those 10 Aβ+ subjects, 7 were MCI/AD and 3 were CN.

Age, diagnostic group, ADmask PiB SUVR, PCC PiB SUVR, ADmask CSFF, and PCC CSFF did not significantly differ between genders, i.e., $p > 0.05$ for all the tests.

Item	Overall	CN	MCI/AD	p-value
Subjects number	21	14	7	-
Gender = M (%)	6 (28.6)	4 (28.6)	2 (28.6)	1
Age (mean (SD))	66.62 (12.58)	64.79 (13.62)	70.29 (11.18)	0.411
Aβ reading status = Positive (%)	10 (47.6)	3 (21.4)	7 (100)	<0.01
ADmask PiB SUVR (mean (SD))	1.58 (0.67)	1.18 (0.16)	2.39 (0.57)	<0.001
PCC PiB SUVR (mean (SD))	1.72 (0.74)	1.3 (0.22)	2.56 (0.69)	<0.001
ADmask CSFF (mean (SD))	5.13 (0.57)	4.85 (0.34)	5.70 (0.51)	<0.001
PCC CSFF (mean (SD))	7.13 (1.01)	6.86 (0.76)	7.65 (1.29)	<0.01

Table 1 Subjects' demographics and clinical information. Last column is the p-value for diagnostic group differences on each measure.

Water maps

Water maps were reconstructed using the 6 TE FAST-T2 data. Figure 1 shows the three water maps of a 72-year-old male with MCI/AD. From left to right are CSFF, IEWF and MWF, respectively. CSFF is defined as CSFF = 100 – (IEWF+MWF) in percent.

CSFF for Aβ deposition

Linear regression between PiB SUVR in ADmask and CSFF controlling for age and gender was performed. Figure 2 presents the partial regression plots between Aβ deposition measured by PiB SUVR in ADmask and CSFF (Figure 2A) and age (Figure 2B). We show in Figure 2A that PiB SUVR is positively associated with CSFF in the linear regression ($t = 5.355$, $p < 0.0001$, $R^2 = 0.609$) and has no association with age ($p = 0.377$) in Figure 2B. According to the plots, a combination of CSFF and PiB SUVR can distinguish most MCI/AD subjects from NL.

CSFF for aging and diagnosis

To investigate the effect of age on CSFF, we performed a linear regression between CSFF and age, gender, and diagnosis. Figure 3 displays the significant relationship between CSFF and age by diagnostic group showing. These data show that CSFF, as a potential biomarker for deficits of glymphatic clearance, increase with age and MCI/AD. Figure 3A is the regression plots between CSFF and age (age: $t = 2.873$, $p<0.01$, Dx MCI/AD: $t = 4.496$, $p <0.001$, $R^2 = 0.618$) controlling for gender. Restricting the analysis for only CN subjects, the regression model still shows a significant relationship between increased CSFF with age ($t = 3.243$, $p < 0.05$, $R^2 = 0.398$), which is consistent with previous results [13]. However, restricting the analysis to only MCI subjects, the CSFF was not significantly associated with age ($t = 1.428$, $p = 0.227$, $R^2 = 0.009$). Figure 3B the boxplot shows a significant difference of CSFF between CN and MCI/AD ($p<0.01$).

Regional CSFF in Aβ positive and negative regions

We performed tests of regional CSFF distribution in Aβ+ and Aβ- regions of the PCC. Figure 4 shows the Aβ+ and Aβ- subregions in the PCC for a 63 years old female CN subject. Figures 4A-4C show the AβpROI and AβnROI masks overlaid on the T1w image in sagittal, coronal, and axial views, and Figure 4D-4F show the same masks on the PiB SUVR image. Figure 5 presents the results of increased CSFF values in AβpROI as compared with AβnROI of PCC by diagnostic group. Figure 5A and 5C are the Bland-Altman plots of the comparison between CSFF in AβpROI and AβnROI subregions, for CN and MCI/AD groups, respectively. It clearly shows that all the points are located within the 95% confidence interval with positive bias, meaning that CSFF in AβpROI region is higher than that in AβnROI region. Figure 5B shows the CSFF changes between AβpROI and AβnROI regions among 14 CN subjects, Wilcoxon Rank test shows that AβpROI region has a higher CSFF than that in AβnROI region ($p < 0.01$). Figure 5D shows the CSFF change between AβpROI and AβnROI regions among 7 MCI/AD subjects. There are 4 MCI/AD subjects with no Aβ- region in the PCC since the PiB SUVR in PCC is greater than 1.6 in all voxels. Consequently, there is no available CSFF in these Aβ- region.

Discussion

Our data demonstrate a significant association between the MR T2 relaxometry-based CSF fraction (CSFF), a hypothesized biomarker of glymphatic clearance, and the PiB PET measured beta-amyloid (Aβ) deposition. Our results show several important findings: 1) Aβ deposition increases with CSFF at the subject level; 2) CSFF increases with normal aging and differentiates CN subjects from MCI/AD; 3) At the voxel level in CN subjects, a higher CSFF

was observed in Aβ+ voxels compared with Aβ- voxels. These results are consistent with preclinical studies that have demonstrated an association between Aβ deposition and deficit of glymphatic clearance. The data points to our novel MRI-based technique as a biomarker for dysfunctional CSF clearance mechanism in AD.

PVS as a glymphatic clearance pathway

Perivascular spaces (PVS), also known as Virchow-Robin spaces, are cavities surrounding the blood vessels in the brain filled with CSF-like fluid [28,29]. The PVS play a crucial role in the brain's waste clearance system, helping to remove excess proteins and other cellular waste products [2,3,30]. Aβ is one of the waste products that is cleared through this system, and its accumulation in the brain is a key pathological feature of AD [1]. The relationship between PVS load and Aβ deposition is still an active area of research yielding mixed results [6,8,31]. PVS enlargement may reflect fluid stasis and reduced flow of CSF through PVS leading to overall deficits in glymphatic clearance [32–34]. Some studies suggest that higher PVS load could be associated with increased Aβ deposition, while others have not found this association [8]. Those mixed results between PVS load and Aβ deposition could result from measurements with insufficient sensitivity to PVS load. Because PVS load segmentation depends on image (typically T2w or T1w) resolution and quality [7,35,36], and only includes the visibly enlarged PVS surrounding periarteries in WM, sub-voxel microscale PVS in both WM and GM are at risk of going undetected despite potentially accounting for the total PVS load in the brain [37,38].

CSFF as glymphatic clearance biomarker for global Aβ deposition

On the other hand, CSFF is a measure of the portion of the voxel that can be attributed to CSF by modeling the MR T2 signal into three water components [13]. This approach of

mapping water fractions was first proposed to map myelin water (MWF) in the brain white matter for multiple sclerosis studies, in which MWF accounts for the short T2 component [9,10,39]. In contrast, CSFF accounts for the long T2 signal component, and theoretically corresponds to the freely mobile water signal, i.e., the CSF (or CSF-like) water. The advantage of CSFF is that it maps all parenchymal CSF water in WM and GM, and could account for CSF in both visible PVS and invisible PVS below the resolution of 3T MRI, and for both periarterial and perivenous spaces. To our knowledge, CSFF is the first biomarker able to detect subvoxel brain CSF water levels in AD rendering CSFF a promising biomarker for early, subtle change of PVS pathology and glymphatic clearance deficits.

Glymphatic clearance deficits are hypothesized to be associated with Aβ deposition due to impaired clearance of Aβ [22,30]. The results show that Aβ deposition is positively associated with CSFF, implying that CSFF has a role in Aβ deposition. As a biomarker, increased CSFF would indicate impaired glymphatic clearance. The strong association between Aβ deposition and CSFF shows the potential of using CSFF to predict Aβ deposition by training a model with large sample. This a topic of our ongoing research.

CSFF for aging and diagnosis

CSF clearance in the lateral ventricle has shown to be associated with aging and imaging markers in AD [5,14]. Although the lateral ventricle bulk flow clearance playa significant role in AD, the flow in tissue on a microscale could reveal more subtle changes in pathology [1]. It has been reported in our previous work that parenchymal CSFF increases with age in CN subjects between the ages of 20 to 80 years old [13]. Those results were replicated in the present study in different a CN subjects depicted as the black regression line in Figure 3A. However, the aging effect trended without reaching significance in MCI/AD group, possibly due to a small sample (n = 7) or high within group CSFF variation. Concomitantly,

our results show that CSFF in MCI/AD subjects is elevated compared with CN when controlling for age and gender, and confirmed by the distance between the red (MCI/AD) and black (CN) regression lines in Figure 3A. Results can be visually confirmed in the boxplots of Figure 3B. Similar findings have been reported in terms of PVS, but only in WM, which is different from our report focusing on the ADmask that samples subregions of the cerebral cortex. It is widely known that PVS segmentation in GM is impossible with standard 3T MRI sequences with poor image resolution. PVS pathology in WM is highly variable due to many factors including small vessel diseases, age, inflammation, and other diseases [40]. This kind of variation in PVS among subjects reduces the specificity of using segmented PVS as a biomarker for early MCI/AD detection.

CSFF correspondence with regional Aβ deposition

Given the advantages of CSFF in GM mapping at the subvoxel level, our regional observation of CSFF and Aβ deposition improves our mechanistic understanding of AD lesion formation. Previous studies have shown that the PCC is probably the earliest region of Aβ accumulation [16–18]. Our data is concordant with that principle given the SUVR of PiB PET in the PCC is higher than in GM. We evaluated Aβ deposition by selecting an early-stage region, the PCC. Results show that in the CN group, the CSFF in Aβ+ subregions of the PCC are higher than in Aβ- subregions, with a a nonsignificant trend was observed in the MCI/AD group. Taken together, the data suggests that CSFF is sensitive to early Aβ deposition. The ability of CSFF demonstrates subvoxel level accuracy of CSF water mapping for microscopic PVS, namely in the cerebral cortex where conventional PVS segmentation methods are not suitable. In MCI/AD subjects, the difference between Aβ+ and Aβ- regional CSFF is not significant, probably due to an overall small sample (n = 7) and because MCI/AD subjects displayed few Aβ- voxels in the PCC.

Limitations of this study

Although the results are promising, the study is not without limitations. First, the study is limited by a small sample size, with 7 MCI/AD and 14 CN subject due to the high standard screening of image quality of CSFF. It is difficult for elderly subjects to remain still during a 90 min scanning protocol, especially for MCI/AD subjects. These results are expected to be confirmed and validated in a larger cohort as part of our ongoing research. An optimization of our scanning protocol is still in development. Third, cross-sectional studies do not reveal longitudinal or causal associations between CSFF and Aβ deposition. We are currently collecting follow-up data on these subjects to further validate the early detection of Aβ deposition using CSFF. Lastly, validation of the association between CSFF and total PVS is not yet established. PVS load segmentation from MR images is limited by resolution that may only include a percentage of the total brain PVS. The validation between these two measures could be performed in histology studies with corresponding MRI scanning in animal models or in post-mortem brain tissue.

Conclusion

We have shown an association between CSFF, an imaging biomarker for glymphatic clearance, and Aβ deposition at both subject and voxel levels. These results provide an improved understanding of the anatomy involved in glymphatic clearance deficits in AD.

Acknowledgements

We thank Drs. Simon Morim, Jonathan P Dyke, Edward K Fung in PET data collection team and Dr. Silky Pahlajani in clinical team for their contributions to this work.

Funding

This study was supported in part by the NIH-NIA grant R01AG057848, R01AG068398, RF1 AG057570 and R56 AG058913.

Competing interests

The authors report no competing interests.

References

1. Tarasoff-Conway JM, Carare RO, Osorio RS, Glodzik L, Butler T, Fieremans E, et al. Clearance systems in the brain—implications for Alzheimer disease. Nat Rev Neurol. 2015;11:457–70.

2. Benveniste H, Liu X, Koundal S, Sanggaard S, Lee H, Wardlaw J. The Glymphatic System and Waste Clearance with Brain Aging: A Review. GER. 2019;65:106–19.

3. Gouveia-Freitas K, Bastos-Leite AJ. Perivascular spaces and brain waste clearance systems: relevance for neurodegenerative and cerebrovascular pathology. Neuroradiology. 2021;63:1581–97.

4. Harrison IF, Ismail O, Machhada A, Colgan N, Ohene Y, Nahavandi P, et al. Impaired glymphatic function and clearance of tau in an Alzheimer's disease model. Brain. 2020;143:2576–93.

5. Li Y, Rusinek H, Butler T, Glodzik L, Pirraglia E, Babich J, et al. Decreased CSF clearance and increased brain amyloid in Alzheimer's disease. Fluids and Barriers of the CNS. 2022;19:21.

6. Kim HJ, Cho H, Park M, Kim JW, Ahn SJ, Lyoo CH, et al. MRI-Visible Perivascular Spaces in the Centrum Semiovale Are Associated with Brain Amyloid Deposition in Patients with Alzheimer Disease–Related Cognitive Impairment. American Journal of Neuroradiology [Internet]. 2021 [cited 2023 Aug 7]; Available from: https://www.ajnr.org/content/early/2021/05/13/ajnr.A7155

7. Sepehrband F, Barisano G, Sheikh-Bahaei N, Cabeen RP, Choupan J, Law M, et al. Image processing approaches to enhance perivascular space visibility and quantification using MRI. Scientific Reports. 2019;9:12351.

8. Banerjee G, Kim HJ, Fox Z, Jäger HR, Wilson D, Charidimou A, et al. MRI-visible perivascular space location is associated with Alzheimer's disease independently of amyloid burden. Brain. 2017;140:1107–16.

9. Nguyen TD, Deh K, Monohan E, Pandya S, Spincemaille P, Raj A, et al. Feasibility and reproducibility of whole brain myelin water mapping in 4 minutes using fast acquisition with spiral trajectory and adiabatic T2prep (FAST-T2) at 3T. Magn Reson Med. 2016;76:456–65.

10. Nguyen TD, Wisnieff C, Cooper MA, Kumar D, Raj A, Spincemaille P, et al. T2prep three-dimensional spiral imaging with efficient whole brain coverage for myelin water quantification at 1.5 tesla. Magnetic Resonance in Medicine. 2012;67:614–21.

11. Bontempi P, Rozzanigo U, Amelio D, Scartoni D, Amichetti M, Farace P. Quantitative Multicomponent T2 Relaxation Showed Greater Sensitivity Than Flair Imaging to Detect Subtle Alterations at the Periphery of Lower Grade Gliomas. Frontiers in Oncology [Internet]. 2021 [cited 2023 Aug 17];11. Available from: https://www.frontiersin.org/articles/10.3389/fonc.2021.651137

12. Daoust A, Dodd S, Nair G, Bouraoud N, Jacobson S, Walbridge S, et al. Transverse relaxation of cerebrospinal fluid depends on glucose concentration. Magn Reson Imaging. 2017;44:72–81.

13. Zhou L, Li Y, Sweeney EM, Wang XH, Kuceyeski A, Chiang GC, et al. Association of brain tissue cerebrospinal fluid fraction with age in healthy cognitively normal adults. Front Aging Neurosci. 2023;Vol. 15.

14. Leon MJ de, Li Y, Okamura N, Tsui WH, Saint-Louis LA, Glodzik L, et al. Cerebrospinal Fluid Clearance in Alzheimer Disease Measured with Dynamic PET. Journal of Nuclear Medicine. 2017;58:1471–6.

15. Zhou, Liangdong, Nguyen TD, Li, Yi. T2 relaxometry based CSF fraction (CSFF) mapping is a better biomarker for brain drainage pathology than DTI-based free water (DTI-FW) mapping. Proc Intl Soc Mag Reson Med. 2022;30.

16. Mosconi L, Rinne JO, Tsui WH, Berti V, Li Y, Wang H, et al. Increased fibrillar amyloid-β burden in normal individuals with a family history of late-onset Alzheimer's. Proceedings of the National Academy of Sciences. 2010;107:5949–54.

17. Insel PS, Mormino EC, Aisen PS, Thompson WK, Donohue MC. Neuroanatomical spread of amyloid β and tau in Alzheimer's disease: implications for primary prevention. Brain Commun. 2020;2:fcaa007.

18. Palmqvist S, Schöll M, Strandberg O, Mattsson N, Stomrud E, Zetterberg H, et al. Earliest accumulation of β-amyloid occurs within the default-mode network and concurrently affects brain connectivity. Nat Commun. 2017;8:1214.

19. Morris JC. The Clinical Dementia Rating (CDR): Current version and scoring rules. Neurology. 1993;43:2412-a.

20. Nasreddine ZS, Phillips NA, Bédirian V, Charbonneau S, Whitehead V, Collin I, et al. The Montreal Cognitive Assessment, MoCA: A Brief Screening Tool For Mild Cognitive Impairment. Journal of the American Geriatrics Society. 2005;53:695–9.

21. Besser L, Kukull W, Knopman DS, Chui H, Galasko D, Weintraub S, et al. Version 3 of the National Alzheimer's Coordinating Center's Uniform Data Set. Alzheimer Dis Assoc Disord. 2018;32:351–8.

22. Butler T, Zhou L, Ozsahin I, Wang XH, Garetti J, Zetterberg H, et al. Glymphatic clearance estimated using diffusion tensor imaging along perivascular spaces is reduced after traumatic brain injury and correlates with plasma neurofilament light, a biomarker of injury severity. Brain Communications. 2023;5:fcad134.

23. Fischl B. FreeSurfer. Neuroimage. 2012;62:774–81.

24. Jenkinson M, Beckmann CF, Behrens TEJ, Woolrich MW, Smith SM. FSL. Neuroimage. 2012;62:782–90.

25. Villemagne VL, Burnham S, Bourgeat P, Brown B, Ellis KA, Salvado O, et al. Amyloid β deposition, neurodegeneration, and cognitive decline in sporadic Alzheimer's disease: a prospective cohort study. Lancet Neurol. 2013;12:357–67.

26. Mosconi L, Rinne JO, Tsui WH, Berti V, Li Y, Wang H, et al. Increased fibrillar amyloid-β burden in normal individuals with a family history of late-onset Alzheimer's. Proc Natl Acad Sci U S A. 2010;107:5949–54.

27. Li Y, Tsui W, Rusinek H, Butler T, Mosconi L, Pirraglia Elizabeth, et al. Cortical Lamina Binding of PET Amyloid and Tau Tracers in Alzheimer's disease. J Nucl Med. 2015;56:270–3.

28. Rudie JD, Rauschecker AM, Nabavizadeh SA, Mohan S. Neuroimaging of Dilated Perivascular Spaces: From Benign and Pathologic Causes to Mimics. J Neuroimaging. 2018;28:139–49.

29. Wardlaw JM, Benveniste H, Nedergaard M, Zlokovic BV, Mestre H, Lee H, et al. Perivascular spaces in the brain: anatomy, physiology and pathology. Nat Rev Neurol. 2020;16:137–53.

30. Jessen NA, Munk ASF, Lundgaard I, Nedergaard M. The Glymphatic System – A Beginner's Guide. Neurochem Res. 2015;40:2583–99.

31. Martinez-Ramirez S, van Rooden S, Charidimou A, van Opstal AM, Wermer M, Gurol ME, et al. Perivascular Spaces Volume in Sporadic and Hereditary (Dutch-Type) Cerebral Amyloid Angiopathy. Stroke. 2018;49:1913–9.

32. Mestre H, Verma N, Greene TD, Lin LA, Ladron-de-Guevara A, Sweeney AM, et al. Periarteriolar spaces modulate cerebrospinal fluid transport into brain and demonstrate altered morphology in aging and Alzheimer's disease. Nat Commun. 2022;13:3897.

33. Kang KM, Byun MS, Yi D, Lee KH, Kim MJ, Ahn H, et al. Enlarged perivascular spaces are associated with decreased brain tau deposition. CNS Neuroscience & Therapeutics. 2023;29:577–86.

34. Ding J, Sigurðsson S, Jónsson PV, Eiriksdottir G, Charidimou A, Lopez OL, et al. Large Perivascular Spaces Visible on Magnetic Resonance Imaging, Cerebral Small Vessel Disease Progression, and Risk of Dementia: The Age, Gene/Environment Susceptibility–Reykjavik Study. JAMA Neurology. 2017;74:1105–12.

35. Lan H, Lynch KM, Custer R, Shih N-C, Sherlock P, Toga AW, et al. Weakly supervised perivascular spaces segmentation with salient guidance of Frangi filter. Magnetic Resonance in Medicine. 2023;89:2419–31.

36. Ballerini L, Lovreglio R, Valdés Hernández M del C, Ramirez J, MacIntosh BJ, Black SE, et al. Perivascular Spaces Segmentation in Brain MRI Using Optimal 3D Filtering. Scientific Reports. 2018;8:2132.

37. Pollock H, Hutchings M, Weller RO, Zhang E-T. Perivascular spaces in the basal ganglia of the human brain: their relationship to lacunes. Journal of Anatomy. 1997;191:337–46.

38. Ineichen BV, Cananau C, Plattén M, Ouellette R, Moridi T, Frauenknecht KBM, et al. Dilated Virchow-Robin spaces are a marker for arterial disease in multiple sclerosis. eBioMedicine. 2023;92:104631.

39. Du YP, Chu R, Hwang D, Brown MS, Kleinschmidt-DeMasters BK, Singel D, et al. Fast multislice mapping of the myelin water fraction using multicompartment analysis of T decay at 3T: A preliminary postmortem study. Magnetic Resonance in Medicine. 2007;58:865–70.

40. Salzman KL, Osborn AG, House P, Jinkins JR, Ditchfield A, Cooper JA, et al. Giant Tumefactive Perivascular Spaces. American Journal of Neuroradiology. 2005;26:298–305.

Figure legends

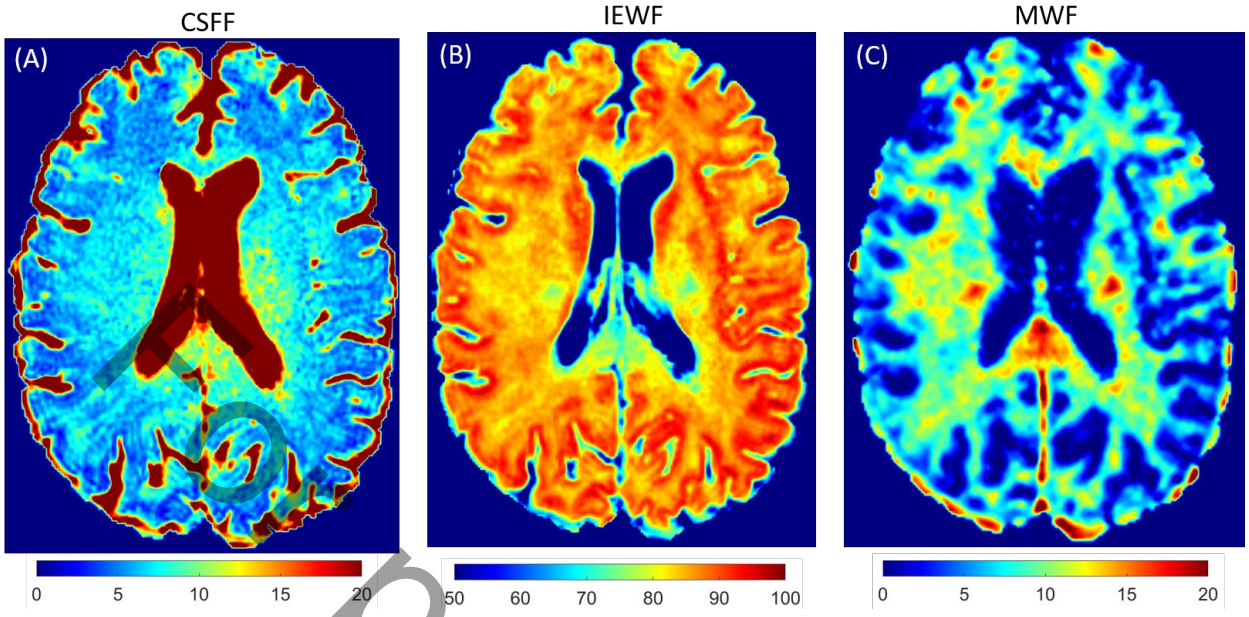

Figure 1. CSF fraction, intra-extracellular water fraction, and myelin water fraction water maps derived from MR FAST-T2 in a 72-year-old, male subject with MCI/AD. (A) CSFF; (B) IEWF; and (C) MWF.

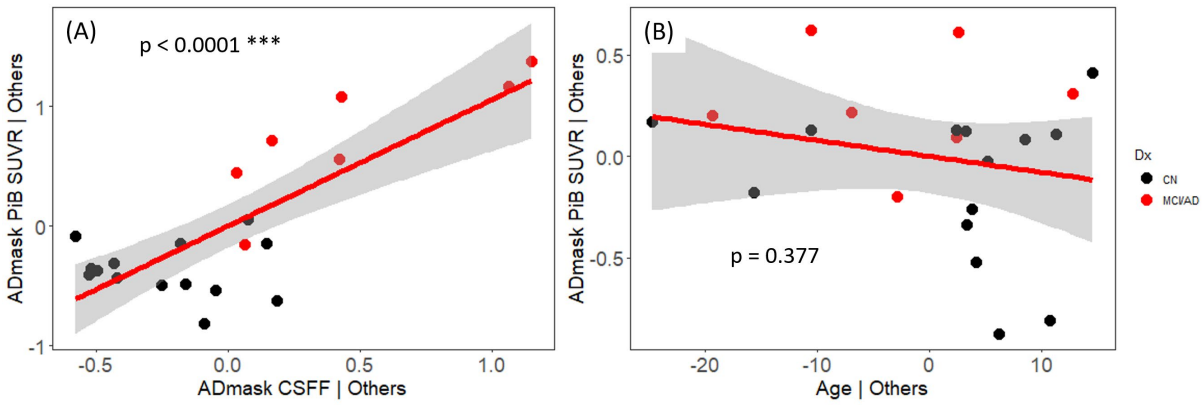

Figure 2. The partial regression plots from multivariable analyses between beta-amyloid deposition measured by PiB PET SUVR in ADmask, CSFF and age. (A) partial regression plots between PiB PET SUVR and CSFF in ADmask ($n = 21$, $t = 5.355$, $R^2 = 0.609$, $p < 0.0001$); (B) partial regression plots between PiB PET SUVR and age ($n = 21$, $p = 0.377$). Black dots represent CN subjects and red triangles indicate MCI/AD subjects. We see that PiB SUVR positively associates with CSFF, and there is no association with age.

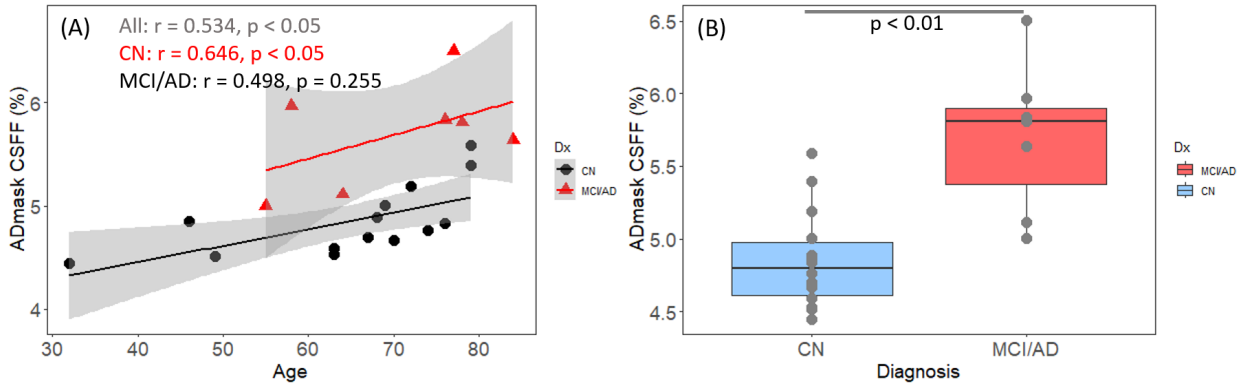

Figure 3. The relationship between ADmask CSFF and age by diagnostic group. (A) the regression plot between CSFF and age by group; (B) boxplot of CSFF by diagnosis. (A) show that CSFF increases with age in both MCI/AD and CN subjects with positive correlation coefficients. There is an elevation of CSFF for MCI/AD compared with CN controlled for age ($p<0.01$). (B) shows significant increase in CSFF in MCI/AD compared with CN subjects.

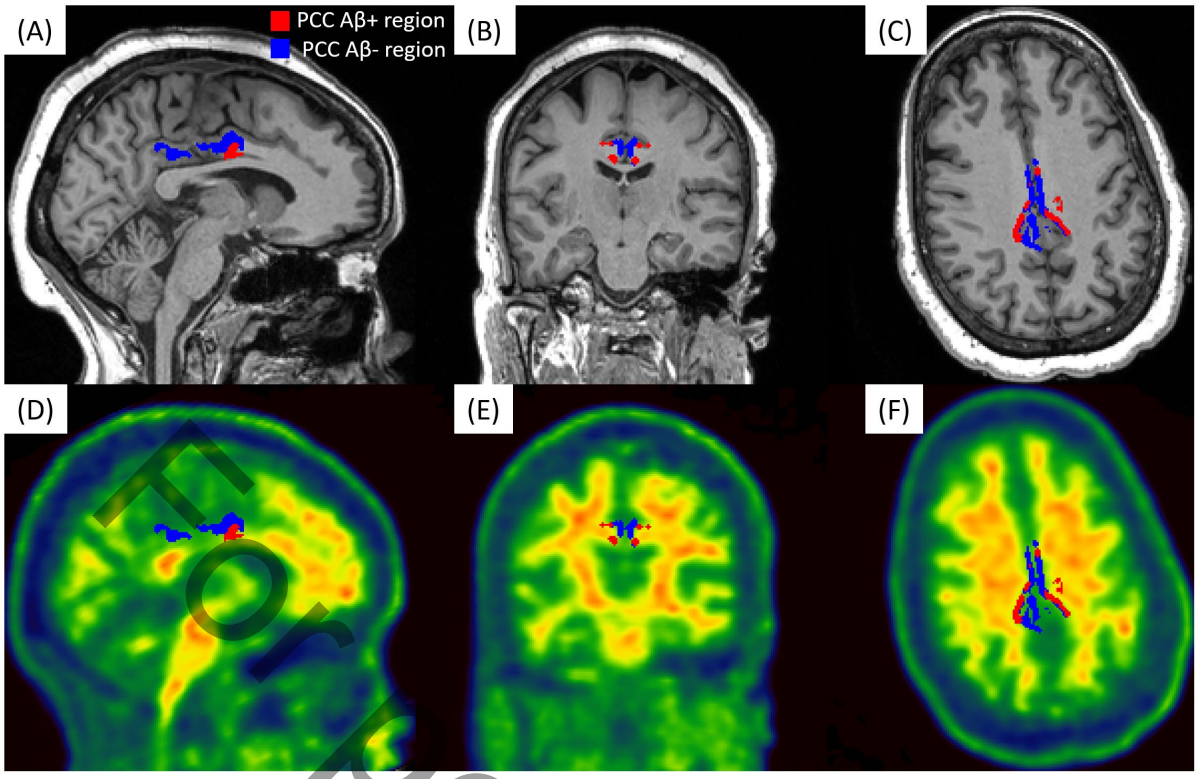

Figure 4. Example of Aβ+ and Aβ- regions in PCC. (A)-(C) are Aβ+ and Aβ- masks on T1w sagittal, coronal, and axial views, respectively; and (D)-(F) overlays of the masks on PiB PET SUVR map. Red color region is for Aβ+ voxels and blue color region is for Aβ- voxels. Please note that the masks were dilated 1 voxel from the outside to enhance the visibility.

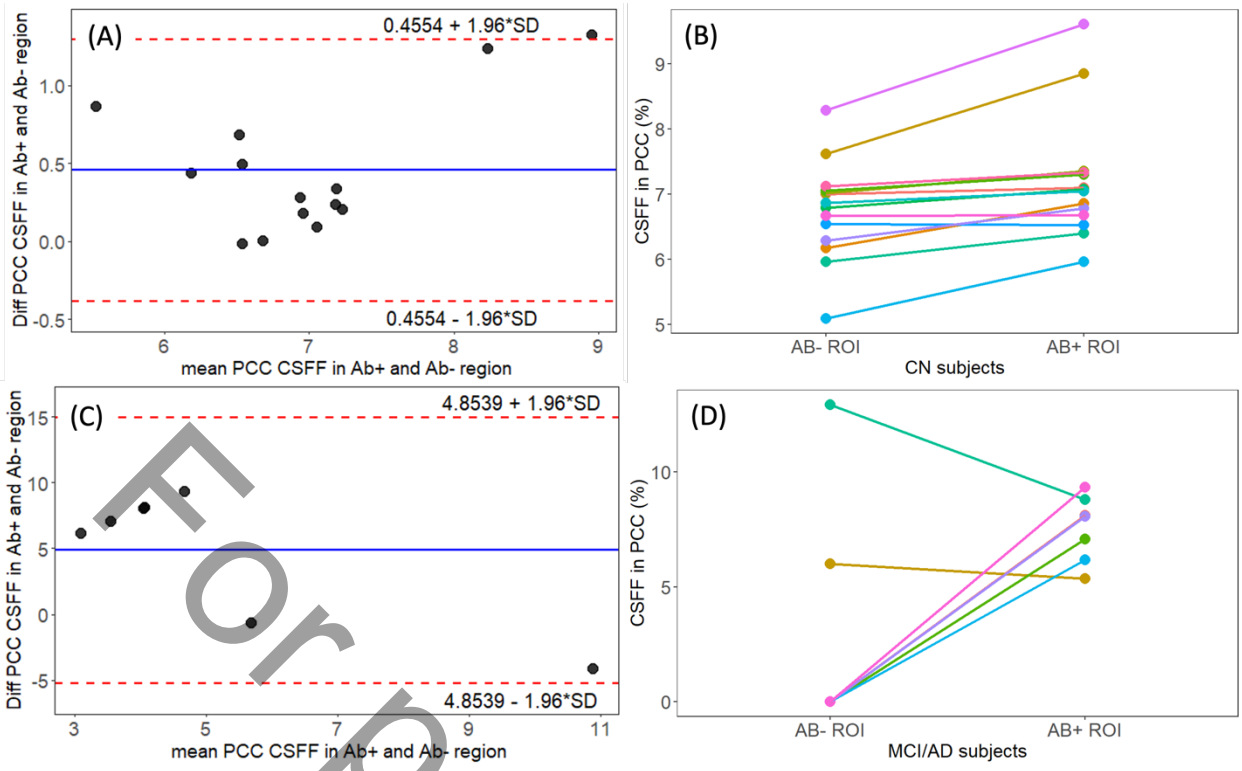

Figure 5 The results of CSFF values in Aβ+ and Aβ- subregions of PCC by diagnostic group. (A) and (B) are plots and comparison of CSFF in PCC Aβ+ and Aβ- subregions for CN subjects. (C) and (D) are plots of CSFF change between in PCC Aβ+ and Aβ- subregions for MCI/AD subjects. In (A) and (C), each point represents a subject. In (B) and (D), each pair of connected points represent the change of CSFF for one subject. We see in CN group, CSFF in Aβ+ regions are significantly higher than that for Aβ- regions.